A Combinatorial MAP Code Dictates Polarized Microtubule Transport

Monroy *et al.*

Supplemental Figures and Figure Legends

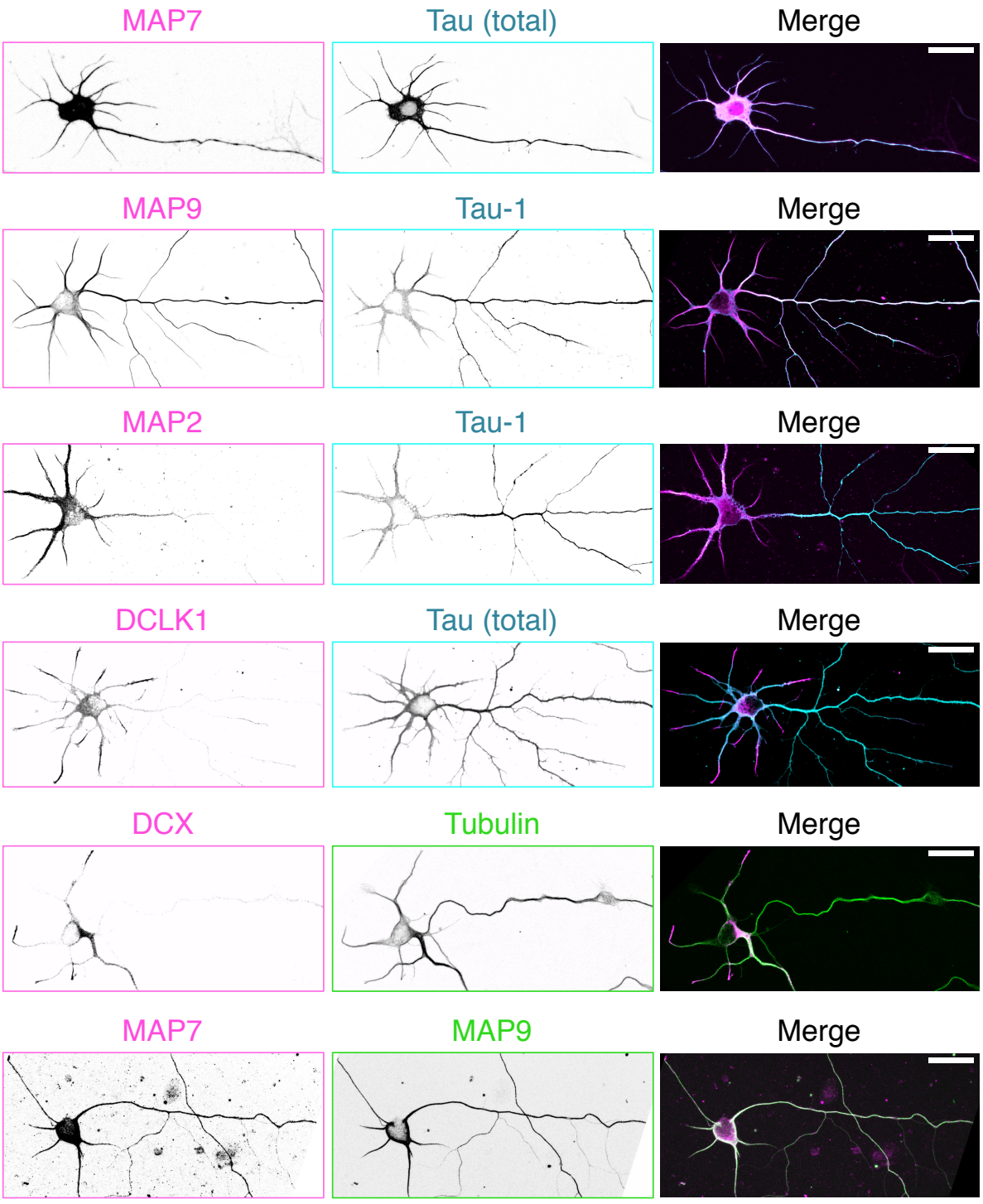

Figure S1. Localization patterns of MAPs in DIV4 mammalian neurons. Related to Figures 1-2. Immunocytochemistry of mouse DIV4 neuronal cultures with antibodies against dephospho-tau (Tau-1), total tau, MAP7, MAP2, MAP9, DCLK1, DCX, and tubulin. Scale bars are 25 µm. n = three independent neuronal cultures for all conditions.

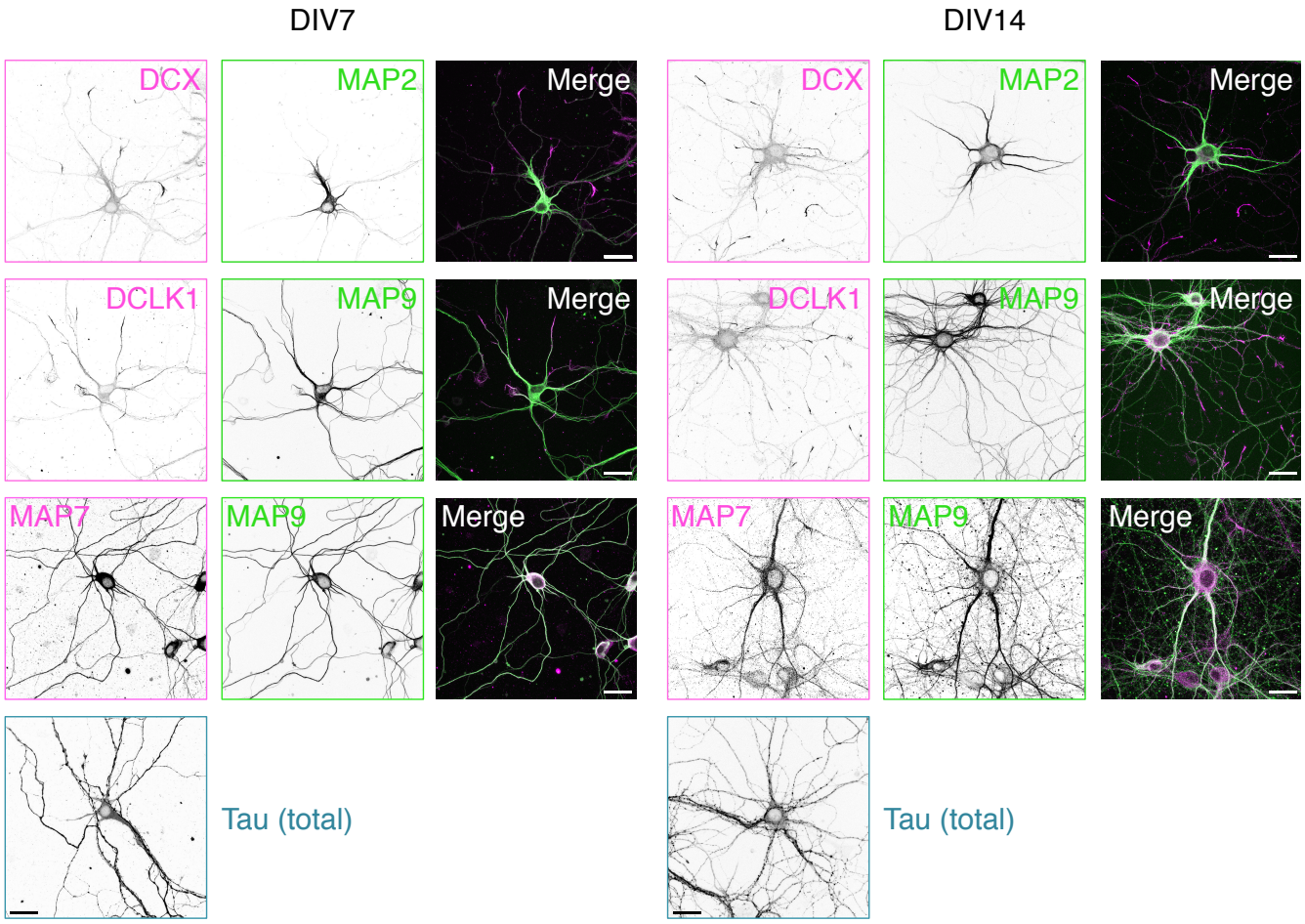

Figure S2. Localization patterns of MAPs in DIV7 and DIV14 mammalian neurons. Related to Figures 1-2. Immunocytochemistry of mouse DIV4 neuronal cultures with antibodies against dephospho-tau (Tau-1), total tau, MAP7, MAP2, MAP9, DCLK1, DCX, and tubulin. Scale bars are 25 µm. n = two independent neuronal cultures for all conditions.

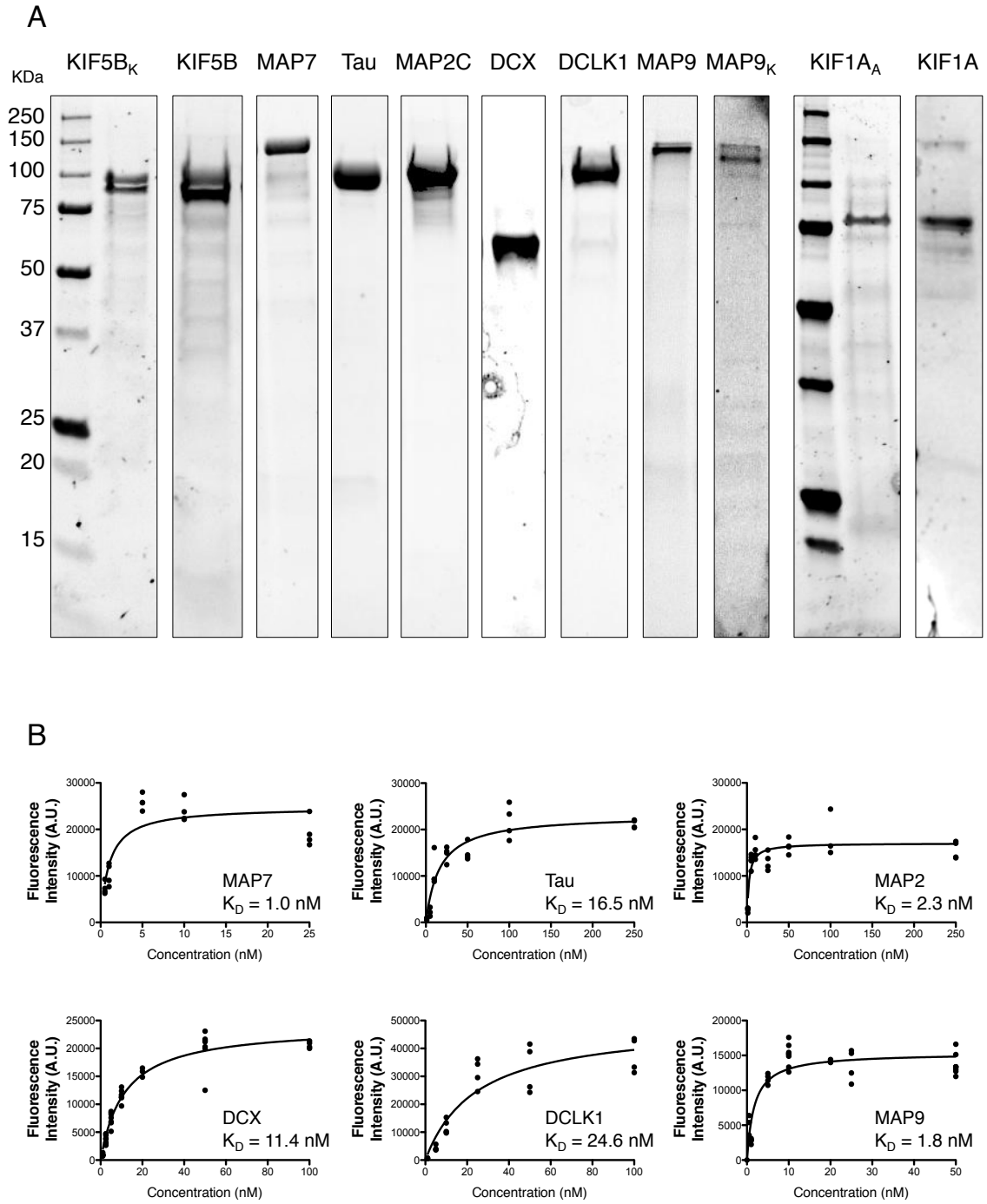

Figure S3. Gels and saturation curves for purified recombinant proteins used in this study. Related to Figures 1-4. (A) Coomassie Blue-stained SDS-PAGE gels of KIF5B$_K$-mScarlet, KIF5B-mScarlet, sfGFP-MAP7, sfGFP-tau, sfGFP-MAP2, DCX-sfGFP, sfGFP-DCLK1, sfGFP-MAP9, sfGFP-MAP9$_K$, KIF1A$_A$-mScarlet, and KIF1A-mScarlet. **(B)** Quantification of fluorescence intensity of microtubule-bound MAPs (all tagged with sfGFP) plotted against concentration. The K_D for each MAP are indicated.

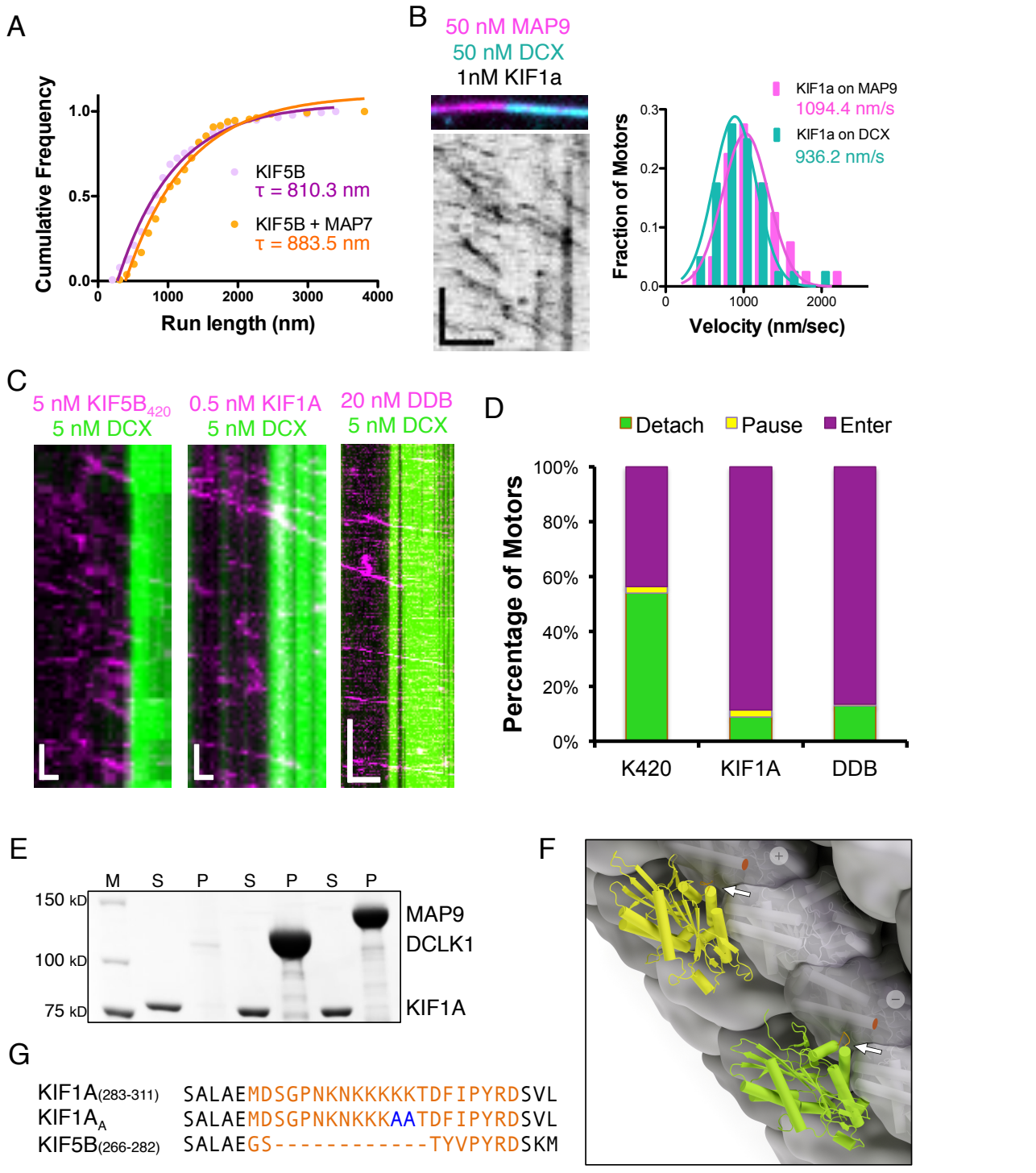

Figure S4. Dissection of the differential molecular effects of MAPs on motors. Related to Figures 1, 2, 3, and 5. (A) Cumulative frequency distribution plot of KIF5B-mScarlet (kinesin-1) run lengths (+ 1 mM ATP) in the absence and presence of sfGFP-MAP7 fit to a one phase exponential decay. τ = 810.3 and 984.3 nm for KIF5B and KIF5B + MAP7, respectively ($P < 0.0001$; n = 138 and 131 KIF5B motors for KIF5B alone and KIF5B + MAP7, respectively, from two independent trials). **(B)** TIRF-M image and kymograph of 1nM KIF1A-mScarlet (kinesin-3) in the presence of 50 nM BFP-DCX (cyan) and 50

nM sfGFP-MAP9 (pink) + 1 mM ATP. Scale bar: 2 μm (*x*) and 5 sec (*y)*. Right: velocity histograms with Gaussian fits of KIF1A motors (+ 1 mM ATP) on MAP9-decorated segments before the MAP9-DCX boundary and on the DCX-decorated segment immediately after the boundary. Means ± s.d. are 1094.4 ± 343.7 and 936.2 ± 321.8 nm/sec for KIF1A on the MAP9 segment and DCX segment, respectively (n = 40 motors that crossed the MAP9-DCX boundary from two independent experiments). **(C)** Kymographs depicting K420-mScarlet (kinesin-1), KIF1A-mScarlet (kinesin-3), and DDB-TMR (dynein-dynactin-BicD) motors encountering a DCX-sfGFP patch. **(D)** Quantification of the percent of K420, KIF1A and DDB motors that detach, pause, or pass DCX patches. For K420 motors, 54.0 % detach, 2.3 % pause, and 43.7 % enter DCX patches (174 events from two independent experiments). For KIF1A motors, 8.7 % detach, 2.6 % pause, and 88.7 % enter DCX patches (115 events from two independent experiments). For DDB motor complexes, 12.8 % detach, 0.7 % pause, and 86.5 % enter DCX patches (133 events from two independent experiments). **(E)** Coomassie Blue-stained SDS-PAGE gel of FLAG pull-downs with purified recombinant proteins. Either full-length sfGFP-MAP9-FLAG or sfGFP-DCLK1-FLAG were used for pull-down assays with KIF1A-mScarlet (n = three independent trials per assay). M = marker, S = supernatant, and P = pellet. **(F)** Visualization of kinesin-3 (KIF1A, PDB: 1i5s; yellow) and kinesin-1 (KIF5B, PDB: 4hna; green) motor domains on the microtubule. Arrows point to loop 12 in orange (KIF5B residues 271-279 and KIF1A residues 288-308; 14 residues of KIF1A, 290-303, are not structurally resolved). Red dots mark C-termini on beta-tubulin, where disordered C-terminal tails are not structurally resolved. **(G)** Sequence alignment comparing loop 12 of kinesin-3 (KIF1A) and kinesin-1 (KIF5B). Sequence of $KIF1A_A$ indicates the two lysines that were mutated to alanines (blue) for the studies in Figure 3A.

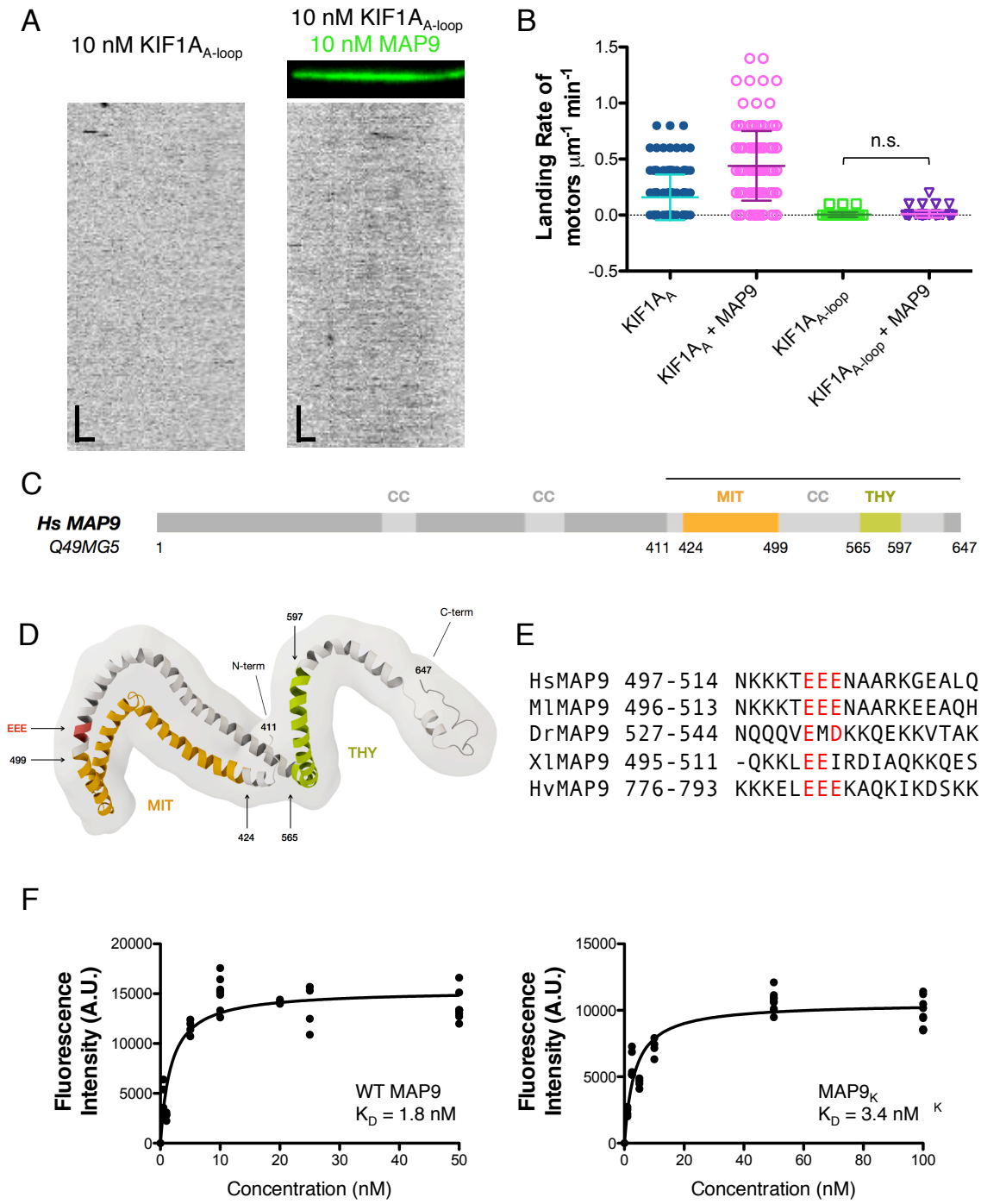

Figure S5. Dissection of the MAP9 interaction with kinesin-3. Related to Figure 3. (A) TIRF-M images and kymographs of 10 nM KIF1A$_{A\text{-loop}}$-mScarlet + 1 mM ATP in the absence and presence of 10 nM sfGFP-MAP9 (green). Images are 10.3 μm wide. Scale bars: 1 μm (*x*) and 5 sec (*y*). **(B)** Quantification of the landing rates of 5nM KIF1A$_{A\text{-loop}}$-mScarlet compared with KIF1A$_A$-mScarlet + 1 mM ATP in the absence and presence of MAP9. KIF1A$_A$ data are reproduced from Figure 3 for comparison. Means ± s.d. for motors μm^{-1} min^{-1} are: 0.005 ± 0.02 for KIF1A$_{A\text{-loop}}$ alone (n = 103 kymographs from two independent trials) and 0.009 ± 0.03 for KIF1A$_{A\text{-loop}}$ + MAP9 (n = 103 kymographs from two independent trials). All datapoints are plotted with lines indicating means ± s.d. *P*

= 0.26 using a student's t-test for $KIF1A_{A\text{-}loop}$ *vs.* $KIF1A_{A\text{-}loop}$ + MAP9. **(C)** Domains and motifs of human MAP9. CC: coiled-coil regions. MIT: microtubule interacting and trafficking domain. THY: thymosin beta actin-binding motif (Venoux et al., 2008). **(D)** Model of the MAP9 C-terminus (aa 411-647), predicted by *de novo* and homology modeling (Buchan et al., 2010). **(E)** Sequence alignment between HsMAP9, *Myotis lucifugus* MAP9 (MlMAP9), *Danio rerio* MAP9 (DrMAP9), *Xenopus laevis* (XlMAP9), and *Hydra vulgaris* MAP9 (HvMAP9). It is important to note that hydra MAP9 is ~300 aa longer at the amino-terminus than human MAP9, thus this region corresponds to the same region of the microtubule-binding domain of human MAP9. **(F)** Quantification of fluorescence intensity of microtubule-bound sfGFP-MAP9 or sfGFP-$MAP9_{EEE>KKK}$ plotted against concentration. The K_D for the wild type and mutant MAP9 proteins are indicated.

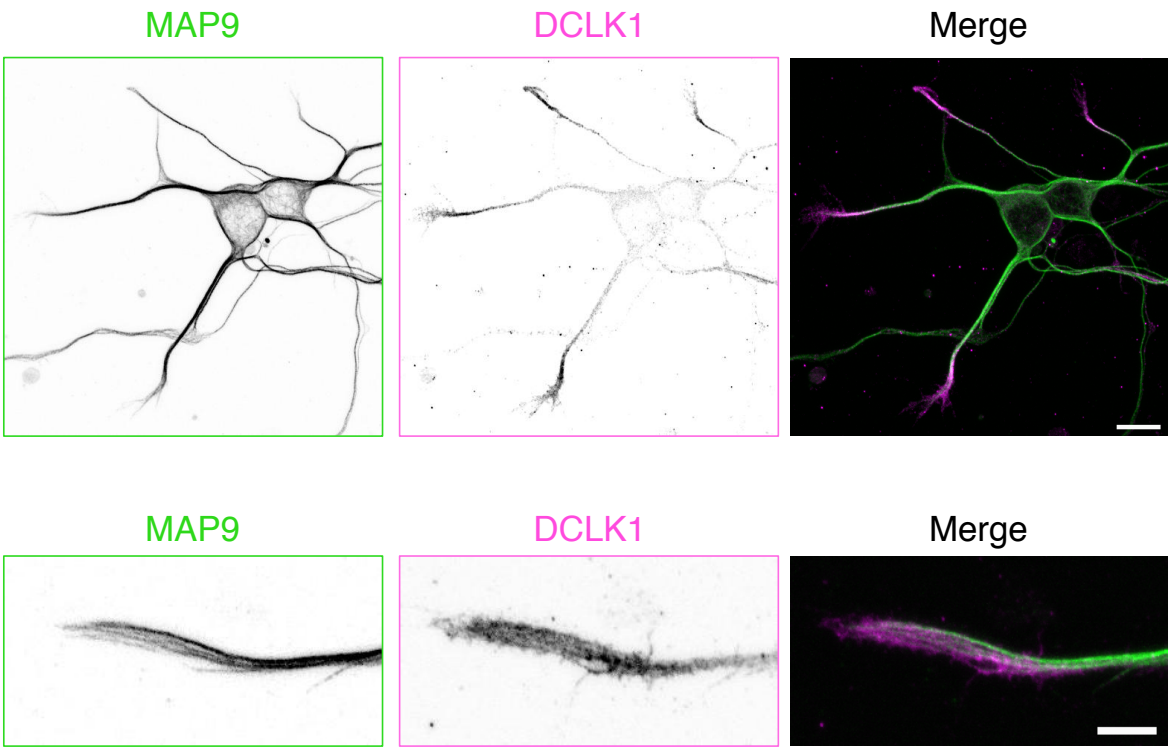

Figure S6. MAP9 and DCLK1 are inversely correlated in distal dendrites. Related to Figure 6. Immunocytochemistry of mouse DIV4 neuronal cultures with antibodies against MAP9 and DCLK1. Scale bars are 10 μm for the large image and 5 μm for the zoomed-in image. n = two independent neuronal cultures.